Universidad Zaragoza

Facultad de Ciencias Universidad Zaragoza

Master Project

Master in Physics and Physical Technologies

Development of a time projection chamber based on Micromegas technology for CAST (CERN Axion Solar Telescope)

Héctor Mirallas Sánchez

mirallas@unizar.es

Facultad de Ciencias, Universidad de Zaragoza

C/ Pedro Cerbuna 12, 50009, Zaragoza, Spain

September 2013

Contents

1. Introduction

I am learning on the laws of nature, on the manner the universe makes itself. I attempt to understand how the probability of to be nothing becomes the probability of to be everything. That is what I take from my lectures, that space and matter are created from something called Big Bang, the very early proof of symmetry break.

While I attempted to learn the laws of macro-cosmos, at the same time, I was introduced on the fascinating world of the micro-cosmos, of the standard model of particles. This theory describes accurately the particles behavior but it looks still uncompleted. One of the problems derived from this theory is that called the strong CP problem, since the theory predicts a symmetry break which is not observed in the experiments.

Axion particle arises in this scenario as solution of the strong CP problem and is greatly accepted among the scientific community, opening many doors to a great number of consequences depending on the characteristics of this particle and its related symmetry.

In the first part of this master project I will make an introduction to the strong CP problem and the Peccei-Quinn solution, whose consequence is the emergence of the axion. We will see briefly its properties, its constraints and how the early universe could have affected the axion production. Then we will see the values of the parameters for which the axion can form the dark matter in the universe. At the end of this first part we will see several experiments in searching for axions, among which the CAST experiment is.

In the second part of this master project I will deal on the CAST experiment exclusively, making an introduction to its components and its techniques. Then I will explain the motivations for working in this experiment which are part too of the whole motivations of the experiment team.

Everything treated until this point has been used as justification of the design and construction of a new detector for the experiment, applying the low background techniques, so the rest of this master project will describe the process of design, mounting and testing of this new detector. We will see the requirements of this detector and the working principle of time projection chambers (TPCs) with Micromegas technology which the detector is based on. We will follow the mounting process and finally we will see the first tests of characterization.

At this moment, earlier of September 2013, the detector is not mounted in the helioscope yet, but it is in process and it is planned to have the CAST ready for taking data for the end of September.

Part I
An introduction to axion world

2. The axion as solution of the strong CP problem

2.1 The strong CP problem

Given the Lagrangian of QCD:

$$\mathscr{L}_{QCD} = -\frac{1}{4}G^a_{\mu\nu}G^{a\mu\nu} + \sum_{j=1}^{n}[\overline{q}_j\gamma^\mu iD_\mu q_j - (m_j q^\dagger_{Lj}q_{Rj} + h.c.)] + \frac{\overline{\theta}g^2}{32\pi^2}G^a_{\mu\nu}\overline{G}^{a\mu\nu} \tag{2.1}$$

$$\overline{\theta} = \theta + Arg(detM) \qquad M \equiv quark\ mass\ matrix \tag{2.2}$$

The first two terms of the Lagrangian in eq. 2.1 are perturbative terms, but the last term contributes through non-perturbative effects associated with QCD instanton (gauge configurations which exist in the QCD vacuum and they are a good candidate to describe chiral dynamics), where G is the gluon field and $\overline{G}$ its dual, g is the strong coupling constant and $\overline{\theta}$ just parametrizes the term's strength.

Non-Abelian gauge theories, e.g. QCD, have a rich vacuum structure owing to the existence of non-trivial, vacuum gauge configurations [1]. The correct vacuum state of theory is a superposition of all the vacuum states $\mid n>$: $\mid \theta> \ = \ \sum_n e^{-in\theta}\mid n>$ where a priori θ is an arbitrary parameter in the theory which must be measured. The state $\mid \theta>$ is referred to as *the θ vacuum*. By appropriate means the effects of the θ vacuum can be recast into a single and additional non-perturbative term in the QCD Lagrangian in eq. 2.1.

If $\overline{\theta}\neq 0$ then that non-perturbative effects violate P and CP.

The best constraints follows from the experimental bound on the neutron electric dipole moment (nEDM) which yields $\overline{\theta} < 10^{-9}$. This nEDM is the most easily observed consequence of QCD, or strong, CP violation.

$$\frac{d_n}{e} = \frac{g_{\pi NN}\overline{g_{\pi NN}}}{4\pi^2 m_N} ln(\frac{m_N}{m_\pi}) \qquad with \qquad g_{\pi NN} = -0.023\overline{\theta} \tag{2.3}$$

The present experimental bound to the electric dipole moment of the neutron, $d_n < 10^{-25}$ e·cm, constrains $\overline{\theta}$ to be so small as pointed out before. The question then is: why is $\overline{\theta}$ so small?

Non-perturbative term in the Lagrangian arises due to two separate and independent effects: the $\overline{\theta}$ structure of the pure QCD vacuum and electroweak effects involving quark masses [2]. In the limit that one or more of the quarks are massless the $G\overline{G}$ term has no physically measurable effects, the θ term can be rotated away by a chiral rotation, and there is no strong CP problem. In the absence of a massless quark species (for which the evidence in our world is strong), the effective $G\overline{G}$ term is made of two unrelated contributions which a priori have no reason to cancel. Namely, in the Standard Model there is no reason why the overall phase of the quark mass matrix should exactly match the value of θ from the QCD sector to yield $\overline{\theta} < 10^{-9}$.

2.2 The Peccei-Quinn solution: the axion emergence

Peccei and Quinn proposed to solve the strong CP problem by postulating the existence of a global $U_{PQ}(1)$ quasi-symmetry [1]. Their idea is to make $\overline{\theta}$ a dynamical variable, which owing to its classical potential relaxed to zero. This is accomplished by introducing an additional global and chiral symmetry, which is spontaneously broken at a scale f_{PQ}. Weinberg and Wilczek realized that because $U_{PQ}(1)$ is spontaneously broken there should be a Goldstone boson: *the axion*. And because $U_{PQ}(1)$ suffers from a chiral anomaly a term in the Lagrangian arises

$$\mathscr{L}_{QCD} \;=\; ... + const\,\frac{a}{f_{PQ}}\frac{g^2}{32\pi^2}G_a^{\mu\nu}\overline{G}^a_{\mu\nu} \tag{2.4}$$

where a is the axion field, *const* is a model-dependent constant and f_{PQ} is the vacuum expectation value which spontaneously breaks $U_{PQ}(1)$. The relation between $\overline{\theta}$ and a follows

$$\overline{\theta} \;=\; \theta + Arg(detM) - \frac{a(x)}{f_{PQ}/N} \tag{2.5}$$

where N is an integer which expresses the colour anomaly of $U_{PQ}(1)$. The non-perturbative effects that make QCD depend upon $\overline{\theta}$ produce an effective potencial $V(\overline{\theta})$ whose minimum is at $\overline{\theta}=0$. Thus, by postulating an axion, $\overline{\theta}$ is allowed to relax to zero dynamically and the strong CP problem is solved.

2.3 Axion properties

A priori the mass of the axion (or equivalently the PQ symmetry braking scale) is arbitrary [1], all values solve the strong CP problem equally well. The axion acquires mass when QCD transition is produced.

The axion mass is estimated as

$$m_a \;=\; 0.6\;eV\;\frac{10^7 GeV}{f_{PQ}/N} \tag{2.6}$$

and the effective Lagrangian for the interactions of axions with ordinary matter [1] is

$$\mathscr{L}_{int} \;=\; i\frac{g_{aNN}}{2m_N}\partial_\mu a(\overline{N}\gamma^\mu\gamma_5 N) + i\frac{g_{aee}}{2m_e}\partial_\mu a(\bar{e}\gamma^\mu\gamma_5 e) + g_{a\gamma\gamma}a\overline{E}\cdot\overline{B} \tag{2.7}$$

where the first term refers to the interaction of axions with nucleons through the coupling factor g_{aNN} which takes the factor g_{ann} for neutrons and g_{app} for protons. The second term refers to the interactions with electrons through g_{aee}. The third and last term refers to the most important interaction in axion searches, as we will see later, that is the interaction with photons through $g_{a\gamma\gamma}$:

$$g_{a\gamma\gamma} \;=\; \frac{\alpha/2\pi}{f_{PQ}/N}(E/N - 1.95) \tag{2.8}$$

where E is the electromagnetic anomaly of the PQ symmetry, $\alpha\simeq 1/137$ is the fine structure constant. In the figure 1 we can see the Feynman diagrams of the interactions mentioned above.

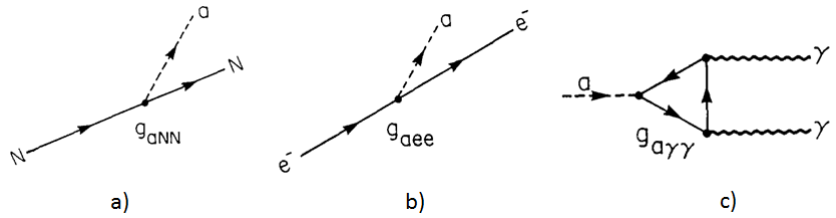

Figure 1. Feynman diagrams for axion couplings to ordinary matter. a) axion-nucleon. b) axion-electron. c) axion-photon.

All the axion couplings (g_{aii}) are proportional to $1/(f_{PQ}/N)$, or equivalently to the mass of the axion m_a. Therefore the smaller the axion mass the weaker the axion couples.

Depending upon the PQ charge of the electron X_e, the axion can be classified as one of two generic types: hadronic where $X_e = 0$ or DFSZ where all the X_i are of order unity.

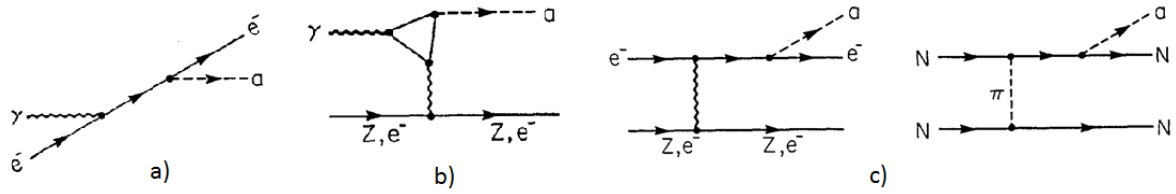

Figure 2. Feynman diagrams for axion dominant emission processes in main sequence stars. a) Compton. b) Primakoff. c) Bremsstrahlung.

3. Axions from outer space

3.1 Constraints from laboratory searches and astrophysics

In the figure 2 can be seen the dominant axion emission processes in stars. For the DFSZ axion the dominant emission processes in main sequence stars, red giants stars and white dwarfs are the Compton like and bremsstrahlung processes. For the hadronic axion the dominant emission process in these objects is the Primakoff process.

Recently, non-minimal axion and ALP (Axion Like Particles) models are receiving increasing attention. For example, non-hadronic axion models such as DFSZ axions have interesting phenomenological consequences. As a contrast to hadronic axions, they couple to electrons at tree level, and this opens additional axion production channels in stars which, as said before, are much more effective than the Primakoff process. In particular, axions with the coupling strength to electrons of $g_{aee} \leq$ few 10^{-13} might explain the long-standing anomaly in the cooling of white dwarfs (WD), recently reinforced by updated studies of the period decrease of the pulsating white dwarf G117 B15A and the WD luminosity function. One should note that this value is already somewhat challenged by the constraint $g_{aee} \leq 2.5 \cdot 10^{-13}$ imposed by the evolution of red giant stars in globular clusters. These values of g_{aee} imply a DFSZ-axion decay constant $f_a \sim 10^9$ GeV corresponding to an axion mass $m_a \sim meV$) and such axions have a wealth of other interesting phenomenological implications in the context of astrophysics and cosmology.

The current state of the standard QCD axion is shown in figure 3. It should be noted that stellar evolution establishes limits on the coupling of axions to radiation, electrons, nucleons, etc., and thus only indirectly limits mass through specific models.

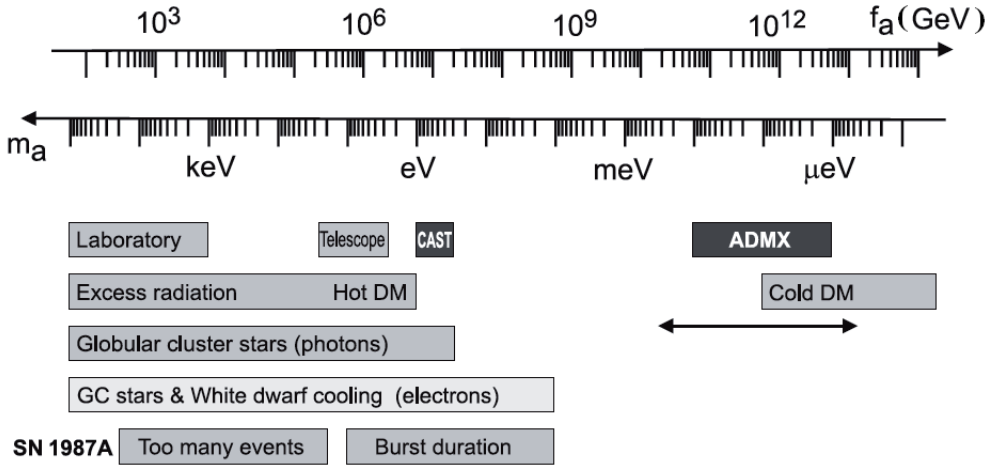

Figure 3. [3] Constraints on the PQ-scale f_a and corresponding m_a from astrophysics, cosmology and laboratory experiments. The light grey regions are most model dependent.

3.2 Axion production in the early universe

Depending on the temperature the axion can be separated as cold axions or thermal axions. Thermal axions, produced by processes as $q+q \rightarrow q+a$ (q is a quark) or $\pi+\pi \rightarrow \pi+a$ (π is a pion), and with a temperature of the same order of magnitude as that of photons or neutrinos, move too fast to constitute the dark matter observed in haloes of galaxies and clusters of galaxies. Cold axions are produce when the axion field settles to the CP-conserving minimum of its effective potential.

3.2.1 Axion field evolution

There are two important scales in dark matter axion production [3]. The first is the temperature at which the PQ symmetry breaks, T_{PQ}. Which of the three mechanisms contributes significantly to the cold axion population depends on whether this temperature is greater or less than the inflationary reheating temperature, T_R. The second scale is the temperature at which the axion mass, arising from non-perturbative QCD effects, becomes significant. At high temperatures, the QCD effects are not significant and the axion mass is negligible. The axion mass becomes important at a critical time t_1, when $m_a t_1 \sim 1$. The temperature of the universe at t_1 is $T_1 \sim 1$ GeV.

As mentioned, the $U_{PQ}(1)$ symmetry gets spontaneously broken at a critical temperature $T_{PQ} \sim f_{PQ}$, where f_{PQ} is the vacuum expectation value of a complex field. At $T > T_{PQ}$ the free energy has its minimum at value of complex field equal to zero. At $T < T_{PQ}$ the minimum of the free energy is a circle, whose radius quickly approaches f_{PQ} as T decreases.

It is well known that the size of the causal horizon is hugely modified during cosmological inflation with a reheating temperature T_R, and regarding the axion field there are two cases to consider: when $T_R < T_{PQ}$ the axion field is homogenized over enormous distances and it has *zero*

momentum mode; in addition, when $T_R > T_{PQ}$ the axion field carries strings and domain walls as topological defects since it has *non-zero modes*.

In an early universe assumed to be homogeneous and isotropic, with a negligible curvature, the space-time metric is as Robertson-Walker metric. The equation of motion for the axion field $a(x)$ in this space-time is

$$(\partial_t^2 + 3\frac{\dot{R}}{R}\partial_t - \frac{1}{R^2}\nabla_x^2)a(x) + m_a^2(t) f_a sin(\frac{a(x)}{f_a}) \; = \; 0 \tag{3.1}$$

The axion mass $m_a(t) = m_a(T(t))$ is a function of temperature hence of time. Because the first three terms in eq. 3.1 are proportional to t^{-2}, the axion mass is unimportant in the evolution of the axion field until $m_a(t)$ becomes of order $1/t$.

3.2.2 Vacuum realignment

When inflation occurs after the PQ phase transition $T_R < T_{PQ}$ with zero momentum mode, the solution of the eq. 3.1 using $R(t) \propto \sqrt{t}$ and $t << t_1$ is shown in eq. 3.2. It implies that the expansion of the universe slows the axion field down to a constant value a_0.

$$a(t) \; = \; a_0 + a_{\frac{1}{2}} t^{-\frac{1}{2}} \tag{3.2}$$

Cold axions will be produced by vacuum realignment [3]. At T_{PQ}, the axion field amplitude may have any value. Non-perturbative QCD effects cause a potential for the axion field. When these effects become significant, the axion field will begin to oscillate in its potential. These oscillations do not decay and contribute to the local energy density as non-relativistic matter. Thus, a cold axion population results from vacuum realignment, regardless of the inflationary reheating temperature.

When inflation occurs before the PQ phase transition $T_R > T_{PQ}$ with non-zero modes, the axion field is spatially varying. This case can be separated in regions of the Universe where axion strings are present as decay of topological defects and free of strings regions.

3.3 The Axion as dark matter candidate

Axions satisfy the two criteria necessary for cold dark matter: (i) a non-relativistic population of axions could be present in our universe in sufficient quantities to provide the required dark matter energy density and (ii) they are effectively collision-less, i.e. the only significant long-range interactions are gravitational. [3]

Luca Visinelli and Paolo Gondolo [4] give the specific values of the theoretical parameters for which the axion can form the totality of cold dark matter. They demonstrate that if the Peccei-Quinn symmetry is restored after inflation, we recover the usual relation between axion mass and density, so that an axion mass $m_a = (85 \pm 3) \cdot 10^{-6}$ eV makes the axion 100% of the cold dark matter. If the Peccei-Quinn symmetry is broken during inflation, the axion can instead be 100% of the cold dark matter for $m_a < 15 \cdot 10^{-3}$ eV. They examined the allowed axion parameter region in the light of data collected at 2009 by the WMAP mission plus baryon acoustic oscillations and supernovae, and assume an inflationary scenario and standard cosmology.

L. Visinelli and P. Gondolo calculated the parameters taking into account only axions produced by vacuum realignment, however decay of topological defects produce too non-relativistic axions which contribute to the dark matter, in a manner that is more difficult to calculate. The confluence of laboratory bounds, cosmological and astrophysical constraints now restrict the QCD axion in mass range, making allowances for uncertainties, of $10^{-6} - 10^{-2}$ eV [5].

With regards to axions as dark matter, independent of the production mechanism, the lower the axion mass, the greater fraction they will claim of the total matter density of the universe. While there is no a priori physics argument favouring a lighter axion to a heavier one, given the inherent uncertainties in the cosmological production, it would be difficult for a light axion not to be cosmologically significant

P. Sikivie and Q. Yang [6] found that gravitational interactions do re-thermalize the axion BEC (Bose-Einstein Condensation) continually so that the axion state tracks the lowest energy state. This is relevant to the angular momentum distribution of dark matter axions in galactic halos. The angular momentum of galaxies is caused by the gravitational torque of nearby galaxies early on when protogalaxies are still close to one another.

Apart from the theories that point to the axion as a good candidate as cold dark matter, others [7] study the dark radiation in the form of relativistic axions, since they rarely interacts with its surrounding and the vast majority of the particles pass through the cosmos unperturbed, leaving a present day population of relic axions which is only diluted by the expansion of space.

4. Axions search

There are currently a variety of experiments searching for axions, whether they are left over from the big bang or produced in stars or the laboratory [2]. Though these experiments search for axions at a variety of mass and coupling scales, most of them rely on the Primakoff process, based on the axion's two-photon interaction, which is described by the following Lagrangian (last term in eq. 2.7):

$$\mathscr{L} \;=\; g_{a\gamma\gamma}\frac{a}{F_a}F_{em}\overline{F}_{em} \tag{4.1}$$

where the axion field a emerges and $F_a = f_{PQ}/N$. F_{em} is the electromagnetic field and its dual $\overline{F}_{em}$ and $g_{a\gamma\gamma}$ is the axion-two photon coupling constant with the relation (see eq. 2.8)

$$g_{a\gamma\gamma} \;=\; \frac{\alpha}{2\pi F_a}\left(\frac{E}{N}-\frac{2}{3}\frac{4+z}{1+z}\right) = \frac{\alpha}{2\pi}\left(\frac{E}{N}-\frac{2}{3}\frac{4+z}{1+z}\right)\frac{1+z}{\sqrt{z}}\frac{m_a}{m_\pi f_\pi} \tag{4.2}$$

where f_π = 93 MeV is the pion decay constant. $z = m_u/m_d \sim 0.56$ is the ratio of quark masses. E and N are the electromagnetic and color anomaly respectively of the PQ symmetry, and in general they are unknown.

Since most of the axion search experiments use Primakof process for treating to catch axions, the general way to compare them is to draw a plot representing the coupling constant in the Primakoff process $g_{a\gamma\gamma}$ versus the mass of the axion m_a. In figure 4 is represented such a plot which includes most of the experiments in search for solar axions and their constrains. The yellow diagonal line represents the zone of theoretical axion models. CAST experiment reaches this zone for

$m_a \sim 1 - 0.1$ eV and microwave cavities reach it for $m_a \sim (2-3)\cdot 10^{-6}$ eV. In both cases the complete range of $g_{a\gamma\gamma}$ for their corresponding masses are not explored. Future IAXO [8] experiment expect to explore a higher range of masses in the models zone.

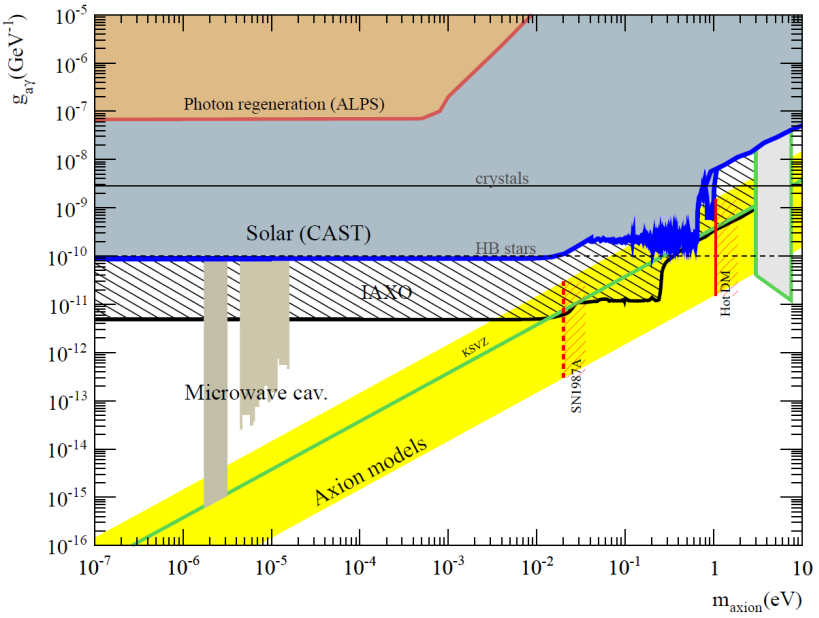

Figure 4. Exclusion limit (at 95% CL) from the CAST phase I and part of the phase II data (^{4}He and ^{3}He up to masses of 0.64 eV), compared to other experimental, theoretical and observational constraints

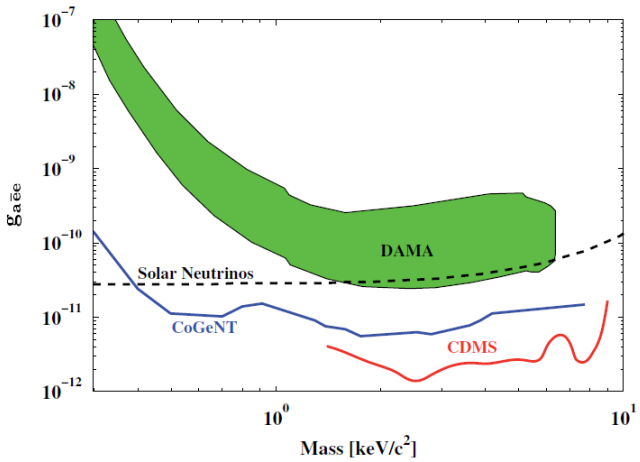

Figure 5. [9] The 90% C.L. upper limit on the g_{aee} coupling constant from this work (red solid line) is shown together with the constraint from CoGeNT experiment (blue solid line). The indirect constraint of pseudoscalar from solar neutrino bound (black dashed line) is shown as well. The allowed region (green filled region) from a galactic axion interpretation claimed by the DAMA experiment is shown for comparison.

An alternative to the most usual axion search was proposed in 1994: use of crystal detectors which meet the Bragg conditions to search for X-rays generated by coherent axion-to-photon con-

version (Bragg diffraction scattering) [2]. Various dark matter WIMP search collaborations were able to look through their data sets and set limits on possible interactions from solar axions. One advantage of this technique is that its sensitivity is independent of axion mass, as long as one can neglect any nuclear recoils.

Normally the axion search experiments, as said most of them based on the Primakoff process, are compared each other by representing the Primakoff coupling $g_{a\gamma\gamma}$ versus the range of the axion mass, as shown in figure 4. Some experiments, as CDMS [9] or DAMA, can look for axion-electron coupling and can be compared by representing of axion-electric coupling g_{aee} versus the range of the axion mass, as is seen in figure 5.

4.1 Laser searches

Laser-based searches are a class of laboratory axion searches that utilize laser photons (γ_{laser}) traversing a magnetic field. Here the polarized laser photons can scatter off virtual photons (γ_v) provided by the magnetic field and convert into axions $\gamma_{laser} + \gamma_v \rightarrow a$. The first technique looks for magneto-optical effects of the vacuum due to polarized laser photons disappearing from the beam as they are converted into axions, and used by PVLAS experiment. The second looks for photons converting into axions in the presence of a magnetic field, which are then transmitted through a wall and converted back into photons by a magnetic field on the other side, so-called light shining through walls experiments or photon regeneration, and it is the case of OSQAR experiment and ALPS experiment.

- OSQAR experiment:

  OSQAR experiment at CERN is aimed to the search of the axions by photon regeneration technique [10]. The experiment is using two LHC dipole magnets of the length 14.3 m and magnetic field 9.5 T equipped with an optical barrier at the end of the first magnet. The flux detection threshold at 95% of confidence level is equal to 0.013 photon/s for the scalar particle search and 0.033 photon/s for the pseudo-scalar particle search (different data taking time and laser intensities). In the limit of massless particles the constraints obtained on di-photon coupling constants are $g_{a\gamma\gamma} < 1.15 \cdot 10^{-7}$ GeV^{-1} for scalar and $g_{a\gamma\gamma} < 1.33 \cdot 10^{-7}$ GeV^{-1} for pseudo-scalar particles.

  The photon regeneration experiment gives negative response until now, no events above the background were detected during data collection, but it can help to extend the exclusion region for axion mass.

- ALPS II experiment:

  ALPS II (Axion-Like Particle Search) experiment at DESY (Deutsches Elektronen-Synchrotron) proposes to combine existing infrastructure at DESY (HERA dipole magnets, long straight sections in the HERA tunnel, cryogenics) with world-leading expertise in laser technology (derived from experience at gravitational wave interferometers) and new optical detectors (superconducting single-photon counters) to achieve sensitivities in WISP searches more than three orders of magnitude better than at existing laboratory experiments [11].

  An optical resonator in front of the wall to “store” the injected laser light and thus to amplify the available laser light power. With a second resonator behind the wall the back conversion

probability of WISPs into photons can be greatly enhanced. The magnetic length is increased by using a string of dipole magnets. As the production of WISPs and the regeneration of photons takes place in a coherent fashion, a 20-fold increase in the magnetic length would result in the same increase in the sensitivity to the WISP-photon coupling strength.

- PVLAS experiment:

  PVLAS experiment is located at the Laboratori Nazionali di Legnaro of INFN (LNL), Padova, Italy (old site) and in the Physics Dept. of the Ferrara University (new site).

  A laser-induced axion-like particle search employing this coupling has been performed since the early 1990s. The setup consists of a sensitive ellipsometer attempting to detect the small changes in the polarization state of light propagating through a 1 meter long magnetic field region in vacuum. It is based on a high finesse Fabry-Perot cavity and a superconducting 5 Tesla rotating dipole magnet [12].

  The experiment team is now setting up a more compact, upgraded prototype in Ferrara. The new ellipsometer is horizontal and the design is based on a pair of permanent magnets. The prototype has already exceeded the performance of the LNL apparatus, and they hope to be able to measure the QED effect quite soon.

4.2 Microwave Cavity

Cosmic axions left over from the big bang may be detected utilizing microwave cavity haloscopes [2]. The strategy relies on primordial axions drifting through a microwave cavity immersed in a strong static magnetic field in which they can resonantly convert to microwave photons. The cosmic axions feeble interactions can be in part compensated by their large numbers, since the number density varies as $\sim F_a^2$ while their cross section varies as $\sim 1/F_a^2$. If the axion makes up the majority of CDM in the Universe, its local density is expected to be roughly 0.45 GeV/cm^3, which yields a number density of $\sim 10^{14}$ axions/cm^3 if one assumes a 4.5 μeV axion. The expected microwave signal will be a quasi-monochromatic line beginning at the microwave frequency corresponding to the axion mass and slightly broadened upward due to the axion virial distribution, with expected velocities of order $10^{-3}c$, implying a spread in energies of $\delta E/E \sim 10^{-6}$.

There could also be an additional signal from non-thermalized axions falling into the galaxy's gravitational well which would yield very sharp signals due to their low predicted velocity dispersion ($< 10^{-7}c$).

- ADMX experiment:

  The Axion Dark Matter eXperiment (ADMX) detects the very weak conversion of dark matter axions into microwave photons [13] and is sited at the Center for Experimental Nuclear Physics and Astrophysics (CENPA) at the University of Washington. Axion conversion into photons is stimulated by an apparatus consisting of an 8 Tesla magnet and a cryogenically cooled high-Q tunable microwave cavity. When the cavity's resonant frequency is tuned to the axion mass, the interaction between nearby axions in the Milky Way halo and ADMX's magnetic field is enhanced. This results in the deposit of a very tiny amount of power (less than 10^{-24} watts) into the cavity.

An extraordinarily sensitive microwave receiver allows the very weak axion signal to be extracted from the noise. The experiment receiver features quantum-limited noise delivered by an exotic Superconducting QUantum Interference Device (SQUID) amplifier and lower temperatures from a ^{3}He refrigerator.

ADMX is sensitive to realistic dark-matter axion masses and couplings and the improved detector allows an even more sensitive search, but no axion signal was found in the mass range 1.98–2.17 μeV [5]. ADMX, beside to CAST, has been able to search in the axion models zone as is shown in figure 4.

4.3 Telescopes/Helioscopes

Axions produced in the nuclear core of the Sun will free-stream out and can possibly be detected on Earth via an axion helioscope. [2] The technique relies on conversion of solar axions into low-energy X-rays as they pass through a strong magnetic field. The flux of axions produced in the Sun is expected to follow a thermal distribution with a mean energy of $\langle E \rangle = 4.2$ keV. The integrated flux at the Earth is expected to be $\Phi_a = g_{10}^2 \cdot 3.67 \cdot 10^{11} \mathrm{cm}^{-2} \cdot \mathrm{s}^{-1}$ with $g_{10} = (\alpha_{em}/2\pi F_a) \cdot g_{a\gamma\gamma} \cdot 10^{10}$ GeV, where α_{em} is the fine structure constant and F_a is the vacuum expectation value which breaks the Peccei-Quinn symmetry. The probability of a solar axion converting into a photon as it passes through a magnet with field strength $\overline{B}$ and length $\overline{L}$ is given as

$$P = \left(\frac{\alpha_{em} g_{a\gamma\gamma} B L}{4\pi F_a} \right)^2 2L^2 \frac{1 - cos(qL)}{(qL)^2} \tag{4.3}$$

Here $g_{a\gamma\gamma}$ is defined as the coupling of the axion to two photons as given in eq. 4.1, while q is the momentum difference between the axion and the photon, defined as $q = m_a^2/2E$, where E is the photon energy. To maintain maximum conversion probability the axion and photon fields need to remain in phase over the length of the magnet, thus requiring $qL < \pi$. For low-mass axions $q \to 0$, leading to a maximum conversion probability. More massive axions will begin to move out of phase with the photon waves though this can be compensated for by the addition of a buffer gas to the magnet volume, thus imparting an effective mass to the conversion photon and bringing the conversion probability back to the maximum. The gas pressure can be varied to tune to various axion masses.

- CAST experiment at CERN:

  The conversion efficiency for axions increases as the square of the product of the transverse magnetic field component and its length [14]. This makes a 9 Tesla, 10 m LHC prototype dipole magnet with two straight beam pipes ideal for the task, giving a conversion efficiency exceeding that of the two earlier telescopes by a factor of almost 100. CAST's LHC magnet is mounted on a platform with vertical movement, allowing for observation of the Sun for 1.5 h at both sunrise and sunset. The horizontal range encompasses nearly the full azimuthal movement of the Sun during the year. The time the Sun is not reachable is devoted to background measurements.

  In order to detect photons coming from the magnet bores, as a result of axion conversion in the magnetic field, several low-background X-ray detectors are installed on both ends of the

magnet. Until 2007, a conventional Time Projection Chamber (TPC) was located at one end, covering both magnet bores, to detect photons originating from axions during the tracking of the Sun at sunset. It was then replaced by two lower threshold and lower background Micromegas (MICROMEsh GAseous Structure) detectors, each attached to one bore. On the other side of the magnet, there is another Micromegas detector covering one bore, and an X-ray mirror telescope with a pn-CCD chip as the focal plane detector at the other bore with pixel size of $145\mu m$, both intended to detect photons produced from axions during the sunrise solar tracking.

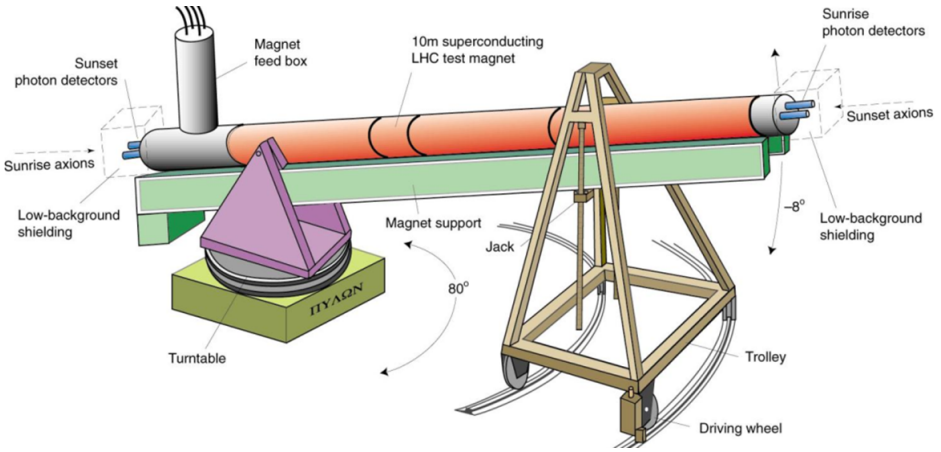

Figure 6. Schematics of the CAST experiment at CERN.

The operation of the CAST experiment was performed in several phases:

Phase I : during 2003 and 2004 the experiment operated with vacuum inside the magnet bores, thus exploring the axion mass range up to 0.02 eV. With the absence of signal over background, an upper limit on the axion-photon coupling constant of $g_{a\gamma\gamma} < 8.8 \cdot 10^{-11}\text{GeV}^{-1}$ at 95% C.L. was set. This result super-seeds the astrophysical limit derived from energy-loss arguments on horizontal branch stars.

Phase II with ^{4}He: in order to extend CAST sensitivity to higher axion masses, magnet bores were filled with a gas. During 2005 and 2006 the magnet bores were filled with ^{4}He. With 160 different pressure settings, the range of axion masses up to 0.39 eV was scanned. The measurement time at each pressure setting was only a few hours, resulting in large statistical fluctuations of the exclusion limit. For the first time, the limit entered the QCD axion model band in the electronvolt rest mass range.

Phase II with ^{3}He: From 2008 to 2011, CAST was taking data with ^{3}He inside the magnet bores and scanned the range of axion masses up to 1.18 eV.

In 2012, CAST has been using ^{4}He in order to revisit, with improved sensitivity and longer exposures, a narrow part of a theoretically motivated range of axion masses around 0.4 eV. In 2013 the experiment is in shut down phase to implement several improvements.

A new helioscope called IAXO (International AXion Observatory) [8] has been purposed for the future which will take into account all the experience accumulated in CAST experiment.

- Tokyo axion Helioscope:

  The Tokyo helioscope search for solar axions with a detector which consists of a 4T x 2.3m superconducting magnet, PIN-photodiode X-ray detectors, and an azimuthal mount to track the sun [15]. The conversion region is filled with cold helium gas which modifies the axion mass at which coherent conversion occurs. In the past measurements, axion mass from 0 to 0.27 eV have been scanned. Since no positive evidence was seen, an upper limit to the axion-photon coupling constant was set to be $g_{a\gamma\gamma} < 6{\sim}10{\cdot}10^{-10}$ GeV (95% CL) depending on the axion masses. The team of the experiment is now actively preparing for a new stage of the experiment aiming at one to a few eV solar axions. In this mass region, our detector might be able to check parameter regions which are preferable to the axion models.

  The Tokyo helioscope uses the same technique than that by CAST experiment at CERN. As shown in the exclusion plot in figure 4, the sensibility of this experiment is minor than that reached by CAST.

4.4 Other approaches

We have seen some the most important axion search experiments among those which are in operation phase, but there are also other approaches for future based on different process: those based on the conversion of axion-like light particle and photon in the intense electric field in crystal [16], using Primakoff process (see figure 7b); based on torsion pendulum that looks for a macroscopic parity and time violating force mediated by virtual axions [17] (see figure 7a); those using resonant radio frequency cavities inserted into dipole magnets from particle accelerators, wiggler magnets developed for accelerator based advanced light sources, and toroidal magnets similar to those used in particle physics detectors [18]; based on the evolution of geomagnetic and terrestrial electric fields, which are coupled by relic axions leaving their fingerprints [19].

Most of this approaches that will be developed in the future, and together to the improvement of those already in operation phase and described before, will mark the axion story, at the same time that theoretical approaches will likely appear to clarify the strong CP problem.

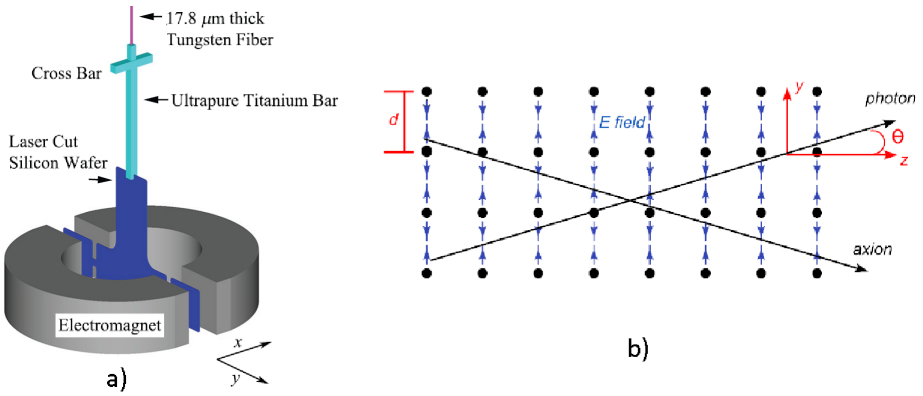

Figure 7. a) A diagram of the pendulum [17]. The gap between the magnet halves is exagerated for clarity. Theinner radius of the magnet was 3 cm, the outer radius of the magnet was 6 cm. b) Axion-like particles photon conversion in intense crystalline field [16]. Plane continuum electric field in y direction is plotted.

Part II
Working in the CAST experiment

5. Previous information on the experiment

The CAST experiment has been taking data since 2003 providing the most restrictive experimental limits on the axion-photon coupling for a broad range of masses. Figure 4 shows the exclusion plot with the recent result compared to other measurements, theoretical and astrophysical bounds.

As said before in section 4.3, when we were speaking about CAST, this experiment uses a LHC prototype dipole magnet with two straight beam pipes. In order to detect photons coming from the magnet bores, as a result of axion conversion in the magnetic field, several low-background X-ray detectors are installed on both ends of the magnet: sunset side and sunrise side.

Until 2007, a conventional Time Projection Chamber (TPC) was located at sunset side, covering both magnet bores, to detect photons originating from axions during the sunset solar tracking. This TPC was a classical development which used copper wires as anode to collect the ions generated at the chamber. Then it was then replaced by two lower threshold and lower background Micromegas (MICROMEsh GAseous Structure) detectors, each attached to one bore, which have the same working principle than a TPC but substituting the anode made of wires by a Micromegas detector which uses the avalanche effect to multiply the ions collected at the TPC (see section 7.2). On the sunrise side of the magnet, there is another Micromegas detector covering one bore, and a X-ray mirror telescope with a pn-CCD chip as the focal plane detector at the other bore, both intended to detect photons produced from axions during the sunrise solar tracking.

5.1 LHC prototype magnet and tracking

In 2003 and 2004 the experiment operated with vacuum inside the magnet (CAST phase I) and set the best experimental limit on the axion-photon coupling constant in the range of axion masses up to 0.02 eV [21] [22]. Beyond this mass the sensitivity is degraded due to coherence loss (for $qL \geqslant \pi$ the sensitivity is reduced owing to the photon-axion momentum mismatch. See eq. 4.3). In order to restore coherence, the magnet can be filled with a buffer gas providing an effective mass to the photon. By changing the pressure of the buffer gas in steps, one can scan an entire range of axion mass values. The CAST experiment started this gas program entering its phase II at the end of 2005. From 2005 to 2007, the magnet bore was filled with ^{4}He gas extending the sensitivity to masses up to 0.4 eV [20]. From March 2008 forwards the magnet bore has been filled with ^{3}He. With the end of the 2011 data taking in July, the CAST experiment had covered axion masses up to 1.18 eV. During 2012 the magnet was filled with ^{4}He for a new scan of axion masses, whereas pressure settings which showed a statistical excess are being revisited for thorough check with more statistics. This analysis is at this moment in progress.

CAST performs periodically the so-called GRID measurements with the help of the team of geometers at CERN. This consists of the independent measurement of the position of the magnet in a set of reference coordinates (GRID) previously defined to cover reasonably all range of movements. These measurements are intended to detect any drift in the pointing ability of the system with respect to the initial calibration values measured in 2002, the ones which are used by the

tracking software to determine the real absolute direction in which the magnet is pointing at any time.

Twice a year it is possible to check the precision with which the magnet is pointing to the Sun, with a direct, visual method. It consists on taking pictures of the Sun in a special Sun filming solar tracking run, with a camera attached to the magnet which was precisely aligned with surveyors help to one bore of the magnet. Also, an atmospheric refraction correction is applied into the vertical motion, because of the difference between axions and photons propagating through the atmosphere.

5.2 X-ray optics

One of the innovations in which CAST success has relied, apart from the availability of a high class magnet like the LHC superconducting test magnet and low background techniques, is the use of X-ray optics to focus the beam and increase the signal-to-noise ratio.

One bore in sunrise side has enjoyed the use of the recycled ABRIXAS spare X-ray optics since the very beginning of CAST, focusing the $\sim$15 cm^2 bore area down to a spot of $\sim$100 times smaller area on the CCD, corresponding to an improvement on the signal to noise ratio of about 50 for that detector. The extension of X-ray optics in number, area and with optimized parameters, has been identified as one of the strategies to pursue for a next generation axion helioscope and is a key component of the IAXO (International AXion Observatory) proposal currently in preparation [8].

The CAST collaboration has the possibility of building one X-ray optics adapted to the CAST geometry and installing it in the Micromegas sunrise line, substituting ABRIXAS. This new optics is one of the main elements of the proposal to operate CAST in 2013-2014. Its implementation in CAST would not only increase the signal-to-noise of the sunrise Micromegas, and the sensitivity of the experiment, but would serve as a pathfinder project to test the technological options being proposed to build large scale X-ray optics with customized parameters for the future IAXO. The building of this optics is delayed and at this moment it is in design phase, and it is planned to be mounted on CAST for the next year.

5.3 Low background techniques

Most of the experiments described before in section 4 are developed on the earth surface and, although it is not necessary to develop them at a underground laboratory, indeed it is necessary in most of them to implement similar low background techniques as used in underground laboratories, as muon veto system, shielding, radio-purity of materials of which the components are made or the control of noble gasses as radon which could came into the detectors.

In laser searches based experiments most of the problems to get a low background are those related to noise. Reduction of the noise needs of specific techniques of vibration isolation and environmental shields. In microwave cavity based experiments as ADMX the goal is to hold a low temperature through cryostatic techniques and temperature shielding.

Helioscopes as CAST and Tokyo use techniques to measure and avoid gamma background, radioactive noble gasses contamination and neutron background. CAST uses a shielding which reduces the background level compared to the detector without shielding [23]: a copper box as Faraday cage to reduce the electronic noise and stops low energy X-rays produced in the outer

part of the shielding by environmental gamma radiation; lead bricks which reduces the low and medium energy environmental gamma radiation; a cadmium layer to absorb the thermal neutrons slowed down by the outer polyethylene wall; polyethylene pieces used to slow the medium energy environmental neutrons down to thermal energies; a PVC bag which covers the whole shielding to flush the inner part with pure N_2 gas in order to purge this space of radon; and a muon veto system mounted in each TPC, at the top of the shielding, to reject muon induced events in the detectors.

CAST has enjoyed the sustained development of its detectors towards lower backgrounds during all its lifetime. The latest generation of Micromegas detectors installed at sunset side has supposed a new step forward in low background, achieving a level of about $1.5{\cdot}10^{-6}$ counts $\mathrm{keV}^{-1}{\cdot}\mathrm{cm}^{-2}{\cdot}\mathrm{s}^{-1}$, a factor 4.5 better that last year detectors and an accumulated factor of more than 100 better than at the beginning of the experiment in 2002.

A new detector and shielding system was proposed for installation this very year 2013 in the sunrise Micromegas line, at the focal spot of the new X-ray optics, following similar design choices as the one done at the sunset side. The design and construction of this new set up has been the goal of this master project.

In addition to that, an upgrade of the muon veto scintillator in sunset side is planned which should further decrease the background down to levels below $1{\cdot}10^{-6}$ counts $\mathrm{keV}^{-1}{\cdot}\mathrm{cm}^{-2}{\cdot}\mathrm{s}^{-1}$. These improvements, together with the new X-ray optics, allow us to consider revisiting the vacuum configuration of CAST with improved sensitivity with respect current CAST limit $g_{a\gamma\gamma}{\leq}8.8{\cdot}10^{-11}$ GeV^{-1} (for $m_a{\leq}0.02$ eV).

Figure 10 shows the computation of the expected sensitivity for 9 months of effective data taking time with the proposed setup, and our current expectations for the background levels. As shown, CAST could improve the current vacuum result down to $g_{a\gamma\gamma}{\leq}5.9-6.3{\cdot}10^{-11}$ GeV^{-1}, corresponding to a factor 4-5 improvement in the detectable signal strength (where the range quoted represents the approximate statistical uncertainty derived from the fact that the expected background counts the new telescope focal area is of only $\sim$1, i.e. in highly poissonian regime). This result would probe deeper into the unexplored ALP region motivated by the theoretical, cosmological and astrophysical arguments (see section 6).

5.4 Detectors

Three Micromegas detectors (one at sunrise and two at sunset) and one pn-CCD chip (at sunrise) are now installed at CAST. Here we will analyse the current Micromegas detectors.

As it is shown in Figure 8, the sunrise Micromegas detector exhibits good performance and stability during all the data taking 2012 campaign, demonstrating a remarkable energy resolution of 15% (FWHM) at 5.9 keV.

A preliminary estimation of the background rate is shown in Table 1, and the background and tracking energy spectra are in Figure 9.

Detector	Background time (hours)	Tracking time (hours)	Background rate [2-7] keV ($\times 10^{-6}$ keV^{-1}cm^{-2}s^{-1})	Tracking rate [2-7] keV ($\times 10^{-6}$ keV^{-1}cm^{-2}s^{-1})
Sunrise	1540	102	5.0 ± 0.1	4.4 ± 0.4

Table 1. Summary of 2012 Sunrise Micromegas results

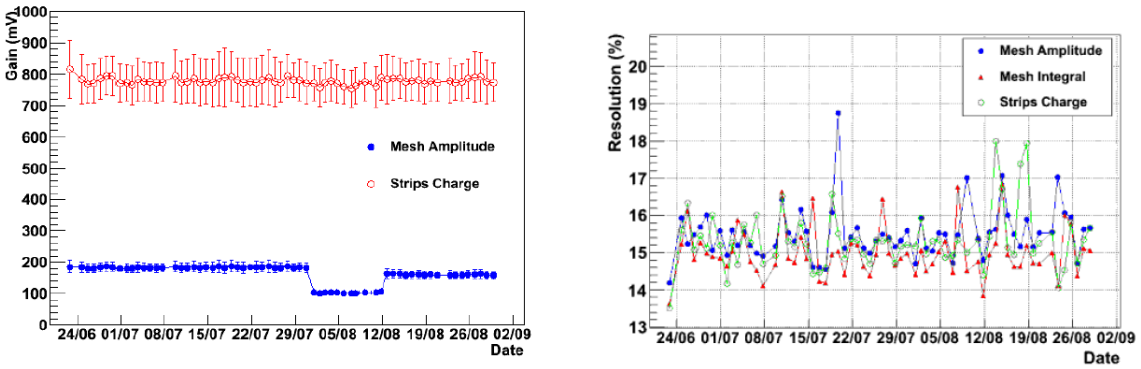

Figure 8. Left: Stability of gain during part of the 2012 data taking. The steps correspond to controlled change of settings. Right: Energy resolutions in terms of FWHM during 2012.

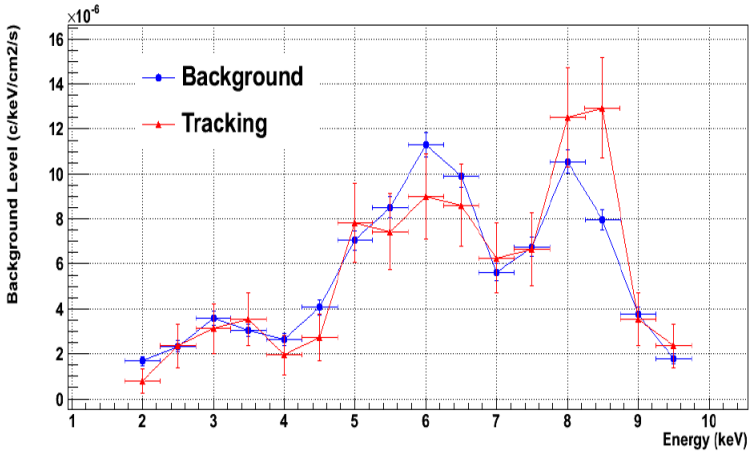

Figure 9. Sunrise Micromegas 2012 background (blue) and tracking (red) energy spectra.

In the sunset side two Micromegas detectors, with better performance with respect to those present in 2011, were installed in 2012. These detectors had a better performance too with respect to those in sunrise side and analyzed above. Moreover, important efforts have been carried out in order to reduce the background level, thus increasing the experiment sensitivity. Main improvements consist in extending the former stainless steel vacuum pipe with a copper one, with the aim of reducing the contribution to background of fluorescence of iron, nickel and chromium (all of them falling in the CAST energy range of interest), and allowing higher solid angle coverage of the lead shielding. A thin PTFE (Teflon®) tube has been installed in the inner part of the new copper

pipe in order to prevent the 8 keV fluorescence from copper. The previous steel cathode has also been replaced by a copper one. The new shielding is made of 1 cm of copper and 10 cm of lead around the detectors. Additionally, a plastic scintillator veto has been installed above the shielding allowing offline rejection of some muon induced background events.

6. Motivations for working in the experiment

As said before, a new detector and shielding system was proposed for installation this very year 2013 in the sunrise Micromegas line, at the focal spot of the new X-ray optics, following similar design choices as the one done in 2012 at the sunset side to reduce the background. The design and construction of this new set up has been the goal of this master project. However, the X-ray optics has not been ready for 2013, and the collaboration team decided to replace only the Micromegas detector and the shielding system to test their behaviour before mounting the new optics.

This master project is a little part of the great efforts that the CAST collaboration team are doing to have the experiment ready to run for 2013-2014. Their motivations, which are too the motivations for this master project, are described bellow.

- IAXO.

  Technologically, CAST has now the possibility to operate in vacuum with increased sensitivity compared with the 2003/04 runs, based on recent ideas and developments which are putting forward in the context of IAXO (the International AXion Observatory) [8], the future axion helioscope whose proposal is under preparation. The tests of these ideas in CAST are per se motivated in view of the IAXO proposal.

- Search for ALPs.

  Although the axion is the best motivated and most studied prototype, a whole category of particles called axion-like particles (ALPs) or, more generically, weakly interacting slim particles (WISPs), are often invoked in several scenarios, theoretically well motivated. ALPs are light (pseudo)scalar particles that weakly couple to two photons, although not within the well known Peccei-Quinn framework associated with the axion. As such, the ALPs parameters $g_{a\gamma\gamma}$ and m_a are now to be viewed as completely independent, and the full parameter space of Figure 10 is potentially populated by ALPs (not constrained to the yellow band as the axion models are).

  ALPs often appear in extensions of the standard model (SM) as pseudo Nambu-Goldstone bosons of new symmetries broken at high energy. But most interestingly, string theory also predicts not just one ALP, but in most cases a rich spectrum of them (including the axion itself). Remarkably, the region of the ALP parameter space corresponding to the first orders of magnitude just beyond the current CAST bound in $g_{a\gamma\gamma}$ correspond to intermediate string scales and are specially motivated as they would contribute to the natural explanation of several hierarchy problems in the Standard Model. It is intriguing that the possible detection of ALPs might become the key to the much sought experimental test of string theory.

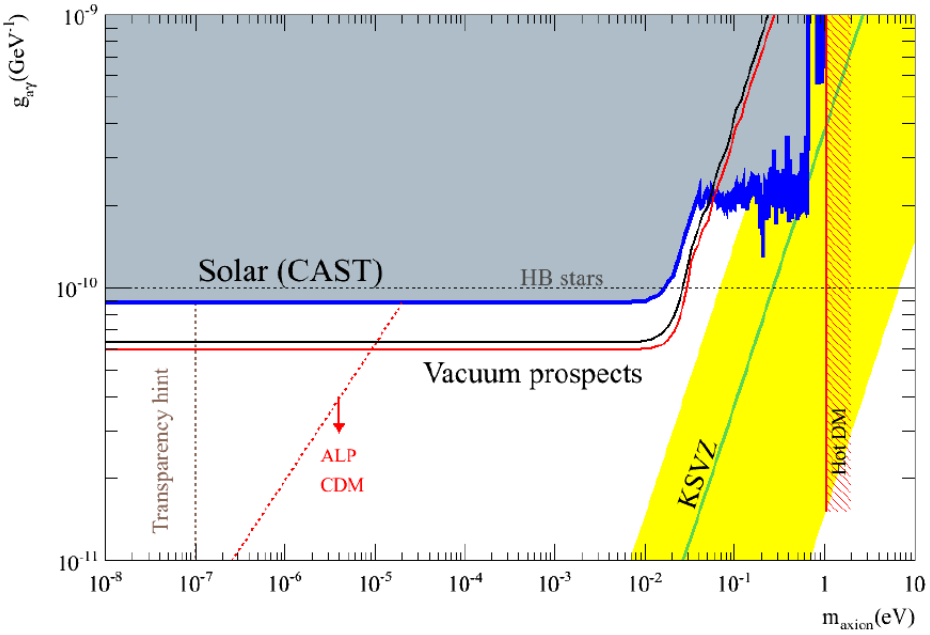

Figure 10. Expected sensitivity with the setup proposed in vacuum conditions 9 calendar months assuming 75% data taking efficiency. Two assumptions in the background for the Micromegas detectors have been computed of $1.5{\cdot}10^{-6}$ (black line) corresponding to a sensitivity of $g_{a\gamma\gamma}{\leq}6.34{\cdot}10^{-11}\text{GeV}^{-1}$ and $8{\cdot}10^{-7}$ counts $\text{keV}^{-1}{\cdot}\text{cm}^{-2}{\cdot}\text{s}^{-1}$ (red line) with a sensitivity of $g_{a\gamma\gamma}{\leq}5.94{\cdot}10^{-11}\text{GeV}^{-1}$. The diagonal red dashed line represents the frontier of the parameter space region in which ALP models with a valid cold DM relic density can be found [24], while the region on the left of the vertical gray dashed line have been invoked in the solution of the Universe transparency problem.

- Search for axions as hot dark matter.

  It is also well known that axions are very good candidates to compose part or all the cold DM of the Universe. However the range of m_a for which axion models can provide all the cold DM density lies below ∼meV, while CAST is currently sensitive to QCD axions only at somehow higher masses ∼0.1-1 eV. In this range the axions would rather contribute to hot dark matter.

- Search for Solar WISPs in the sub-keV range.

  CAST baseline configuration in the past has been optimized for the detection of X-ray photons of 2-10 keV energies coming from the primary, more generic, source of axions in the Sun: the Primakoff conversion of solar plasma photons. Some non-standard scenarios predict emission of WISPs by the Sun in this energy range, being the BCA axion emission a good example. Another very relevant example are solar chameleons. These models have been proposed in the context of particle interpretations of the nature of dark energy. Recently it has been noted that they could also be produced in the Sun with sub-keV energies, being potentially detectable by helioscopes.

  Independently of the theoretical framework behind, the proposed experimental improvement of CAST will open a completely new observational window for WISPs in the sub-keV range,

previously unexplored. It is considered the possibility of using such a unique setup like CAST, enhanced with sensitivity in a new energy window, is by itself worthwhile pursuing.

Beyond the dark matter problem, which could be solved by theoretically motivated particles such as axions and WIMPs, the problem of the dark energy lacks however such well-motivated solutions. The greatest mystery in modern cosmology is the origin of the accelerating expansion of our universe, suggesting either some negative-pressure substance, dubbed dark energy (DE), or a modification to the theory of gravity on the largest length scales. Either explanation involves "new physics", some of which can be investigated in parallel with dark matter by using existing experiments in astroparticle physics and other disciplines.

7. Designing a new detector

7.1 Requirements

The changes that produced an improvement near to a factor 4 in Sunset Micromegas (SSMM) background, with respect to Sunrise Micromegas (SRMM), will be applied here together with some further innovations.

As was done in SSMM: the replacement of steel pieces with PTFE (Teflon®) or copper, especially the piece of the pipe closest to the detector; the use of PTFE foils to minimize the 8 keV X rays fluorescence of copper; the reinforcement of inner copper shielding, the minimization of the signals extraction outlet; the enlargement of the lead external shielding. The last issue, certainly of great importance, depends on final studies of the available space (which depend as well on the final chamber design) and the tolerable load on the platform. A lead external shielding of 10 cm thickness, as in SSMM, is the baseline value, and cannot be less than 5 cm thick.

Some advantages with respect to present SSMM will be the use of a smaller window, thanks to the X-ray optics. The radio-purity of the set up will also be improved with the use of PTFE home-made vacuum gaskets instead of the typical Viton® ones. Finally, as for the SSMM, a specifically designed cosmic veto will be installed.

The ultra low background goal imposes both the material selection according to radio-purity and the geometry defined by the shielding. Other design criteria for this set up such as modularity and flexibility have been taken into account.

The presence inside the detector of non-radiopure materials has been avoided or reduced as much as possible. Besides, epoxy candidates used to bind the aluminized PET to the cathode such as Ellesworth Hysol® and Henkel Stycast® have been bought in large quantities to be measured with a Germanium detector in LSC (Laboratorio Subterráneo de Canfranc) to quantify their effect.

7.2 TPCs based on Micromegas technology

Micromegas technology is applied on last class detectors used at particles physic experiments [25]. It is made up of two zones separated by a micro-grid or mesh: conversion zone and amplification zone (see figure 11). At the conversion zone the photons ionize the gas inside the TPC volume, and these ions are collected by the electric field towards the mesh. At the amplification zone, when the ions collected at the conversion region came in this zone, the avalanche effect is produced thanks to the high electric field applied between the mesh and the anode. The electrons produced by

the avalanche effect are collected in the tracks sited on the anode, and then a measurable electric signal appears in the tracks which gives information on the deposited energy and on the spatial distribution. The ions produced by the avalanche effect are collected on the mesh, yielding another measurable electric signal which will be used by the electronic device to initiate the reading of each event.

Length of conversion zone depends on the trace length produced by the ionization of photons in the gas contained at the TPC volume, and the electric field is up to 1 kV·cm^{-1}. Length of amplification zone is 50-150 μm, and the electric field is $\sim$100 kV·cm^{-1}.

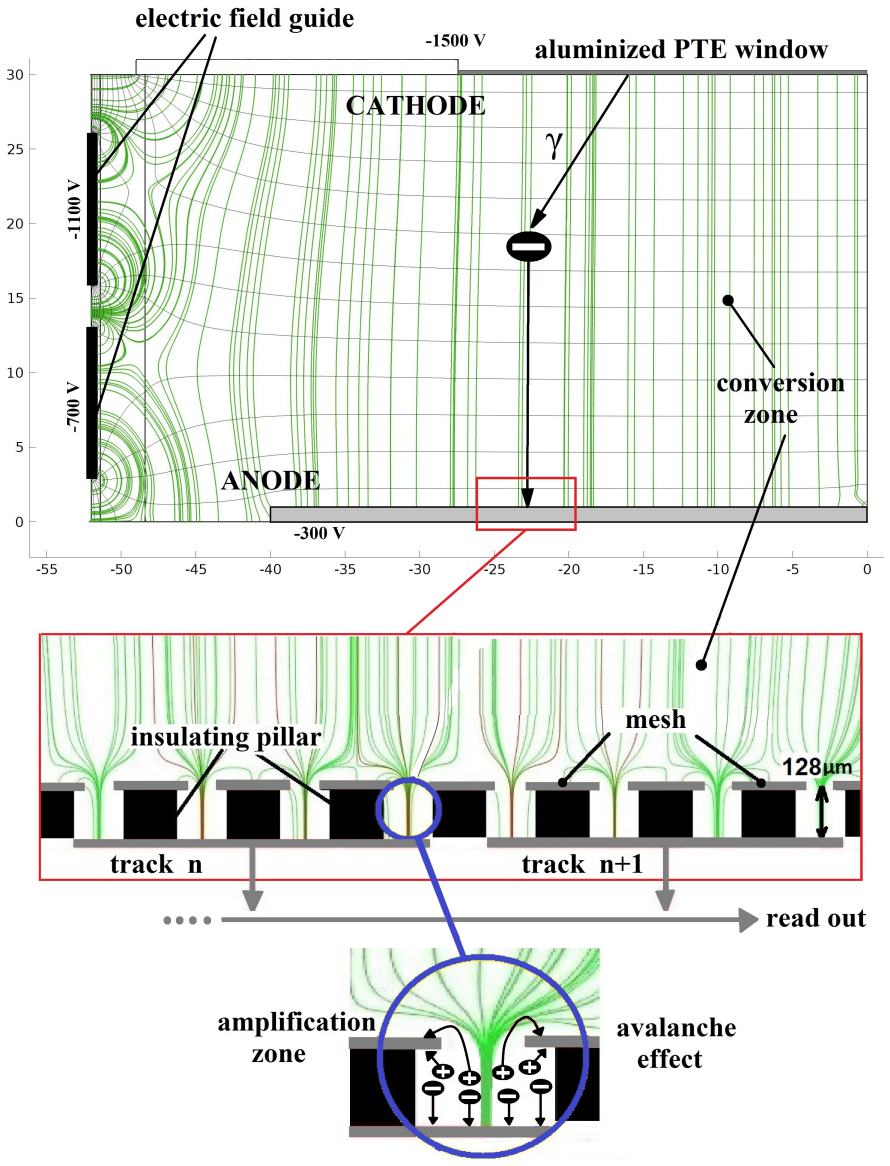

Figure 11. TPC section with Micromegas detector. Conversion zone where gas is ionized. Amplification zone where electrons are collected to the tracks and ions are collected to the mesh.

7.3 New detector TPC design

Figure 12 shows the three main parts of the detector copper shielding and chamber: the interface which connects the detector with the magnet pipe, the vessel body (with Argon ports, cathode and electric field guide inside), the copper racket with the Micromegas printed circuit glued on it and the pins of the electrical field guide in contact to the circuit through a bracket screwed to the racket.

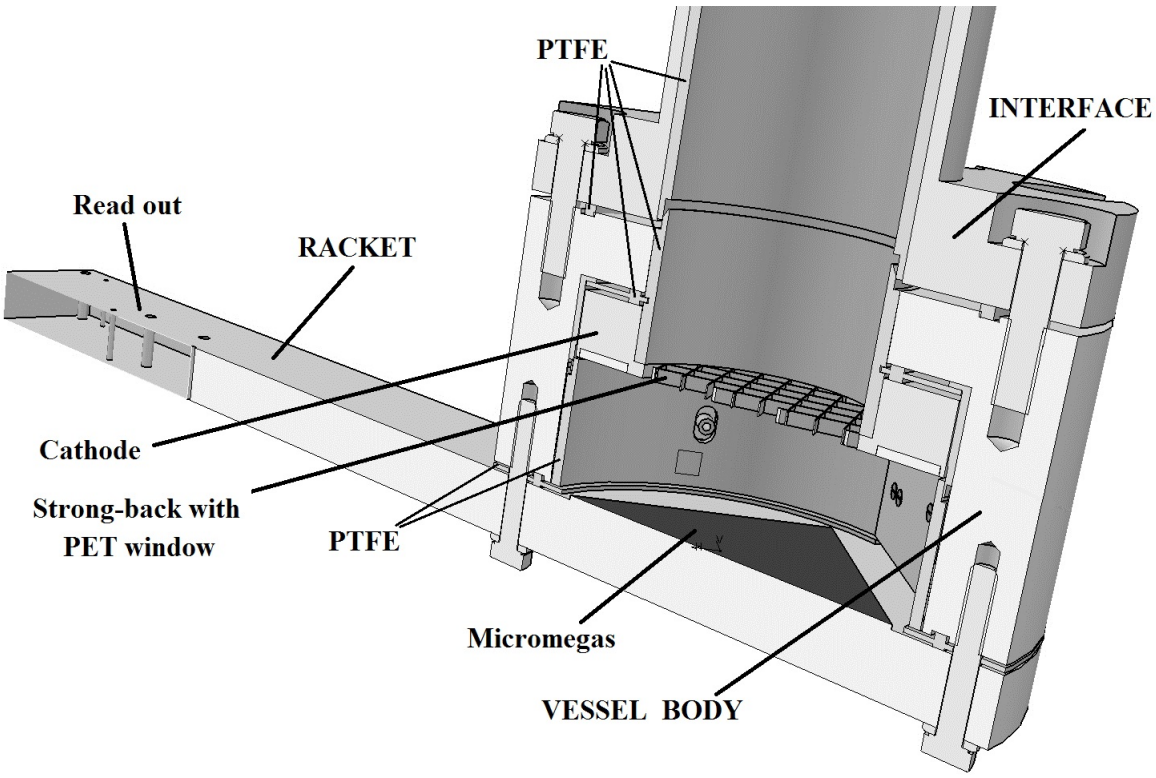

Figure 12. General overview of the new detector. It can be seen the three most important zones: the interface which connects the detector with the magnet pipe, the vessel body with the TPC and the copper racket with the Micromegas printed circuit glued on it

Now a detailed description of the new detector elements:

1. **The interface tube**: This piece must provide some flexibility, so that any possible change in the detector (focal length modification, lead shielding dimensions variation because of weight constrains, etc.) is absorbed by a new design of the interface.

   Two PTFE cassettes with a wall thickness of 3 mm are inserted inside the tube in order to shield the copper fluorescence of 8 keV peak and to isolate the cathode electrically.

   The Vacuum level of 10^{-5} mbar is assured by eight M8 copper bolts and a PTFE gasket.

2. **The vessel cylinder**: This is the core of the design. This shape machined from a billet minimizes to two the number of gaskets required to seal the chamber and makes easy the assembly with the interface tube. Moreover, it includes the gas ports and holes inside to fit the PTFE cassettes with the electric pins embedded.

3. **The cathode**: The cathode has a strong-back for the aluminized PET with 6mm sided squared holes obtained by means of electro-erosion. There is a central hole through which the converged ray of the telescope should pass.

4. **The electric field guide**: In order to optimize the usage of volume inside the chamber, a design of the electric field guide based on a flexible printed circuit is preferred over a design based on copper ring and plastic columns. The electric field guide is a single layer flex circuit with Polyamide (PI) as substrate.

   A study of the electric field inside the chamber was performed and 2D simulation, using finite element method, were developed in which the electric field and equipotential surfaces, at different critical planes of the electric field guide, are considered. The figure 11 shows the electric field simulation of the selected and final configuration for the electric field guide.

5. **Sealing**: The sealing between vessel cylinder and copper racket modules is performed by a standard PTFE gasket. Its dimensions and torque applied to the bolts have been already calculated though EN norms. Since there cannot be any electric sparks between the cathode (up to 1500 V) and the chamber walls (Ground), the gasket chosen has a peculiar shape that ensures the cathode isolation.

   Some tests were carried out in order to check the vacuum achieved with this home-made gaskets with very promising results, with a Helium leak rate of $< 10^{-12}$ mbar·l/s and a vacuum value of 10^{-5} mbar after five minutes pumping at Zaragoza Laboratory installations.

   The set up was kept mounted in atmospheric conditions (with the flanges bolted) and two months later the vacuum level of this set up was tested once again with the same results: 10^{-5} mbar after five minute pumping. Thus, it is considered that the effects of creep deformation cannot ruin the gas tightness of this sealing.

7.4 Electronics

7.4.1 Micromegas circuit

The design of the detector circuit is shown at figure 13. There are two main parts, the active area inside the chamber, and the neck with routing of High Voltage and signal connection. The flexible board has three layers: Top (with Mesh, Rim, HV routing and pins connection so as to signal Samtec® pads), Inner (with pixels in active area and hatched ground outside active area which provides shielding between signal and HV routing) and Bottom (with signal routing from active area to Samtec® pads).

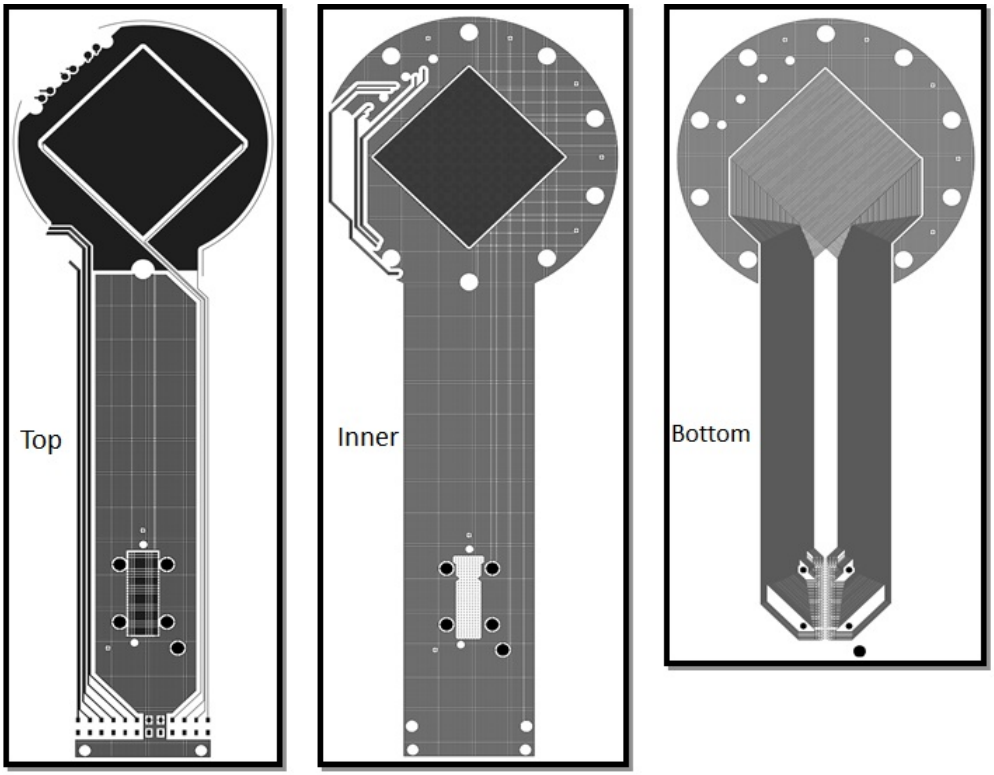

Figure 13. Detector circuit with the layers Top, Inner and Bottom.

As explained in section 7.2, Micromegas detectors are based on the avalanche effect produced at a space with a high electric field. The detector for the experiment has an active area of 60 x 60 mm (see figure 13), containing 120 x 120 tracks (bottom layer) which collect the signal produced by the avalanche (see figure 11).

7.4.2 Read out

The signal produced by the avalanche and collected by the tracks in the circuit must be recorded for post-analysis. The read out system was developed for the TPC of the T2K experiment (Tokai-to-Kamioka) [26]. The CAST experiment uses a FEC (Front-End Card), a FEM (Front-End Mezzanine) and a DCC (Data Concentrator Card). This system is based on the integration of the chip called AFTER at the FEC cards, which amplifies y digitalizes the signal coming from each track of the Micromegas and records them in 511 temporal channels (time bin).

Each FEC contains 4 AFTER chips with a total of 288 read out channels. In this case only 240 channels are going to be used, corresponding to the 120 + 120 tracks at the Micromegas circuit. The FEM card recovers the data coming from the FEC card and sends them to the DCC card by optical fiber. The DCC card sends the data to any PC connected to an ethernet network. In the PC all the data are uploaded for a post-analysis.

Figure 14. Cleaning process. Soap Cleaning and Acid Etching.

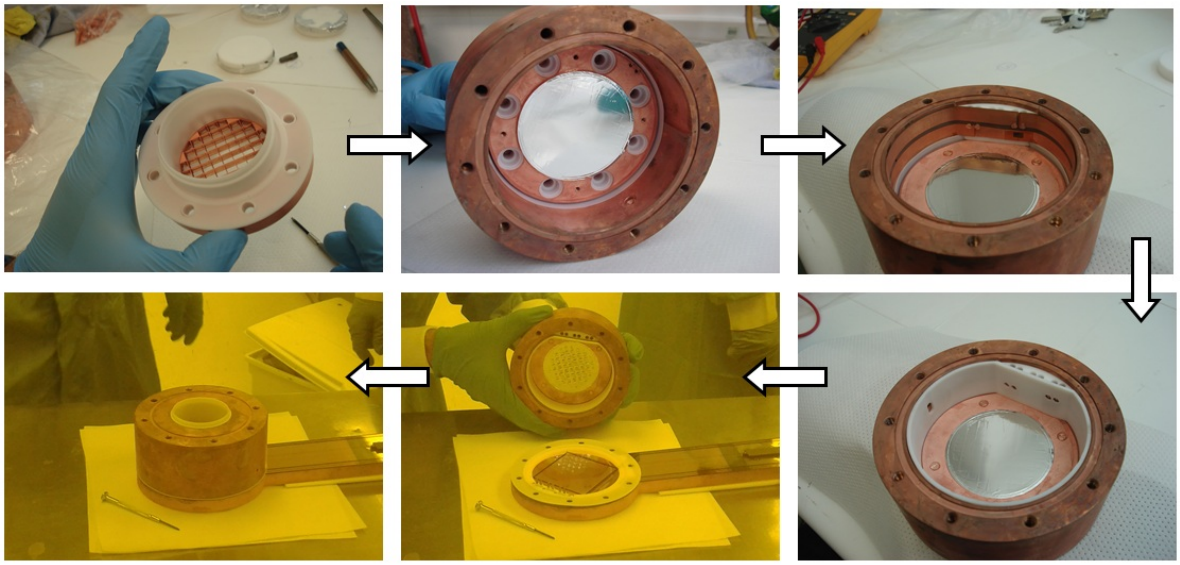

Figure 15. Photos succession of Assembling process: cathode gasket adjustment, cathode-chamber adjustment, electric field guide positioning, PTFE cage covering the field guide, chamber being attached to the rascket with the Micromegas circuit and detector completed.

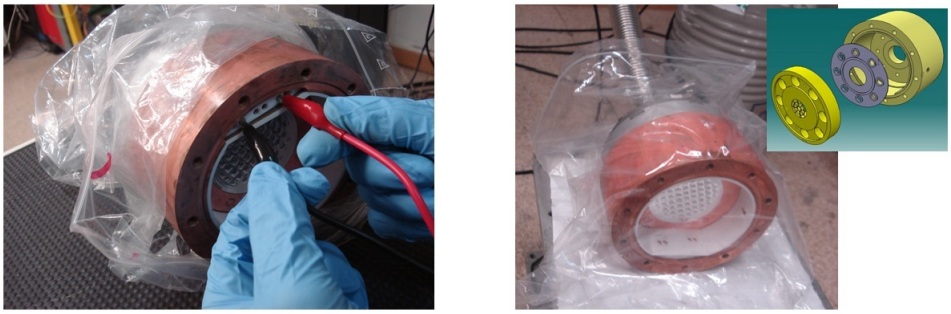

Figure 16. Photos of Impedance measures and vacuum test.

8. Mounting and testing the new detector

8.1 Cleaning

After the fabrication of the parts is necessary to clean them to remove all the impurities which have been deposited at the surface during the production process and their manipulation, otherwise this impurities could contain radioisotopes which could influence negatively in the background. Let remind the importance of the radio-purity of the materials. This process is divided in two steps:

1. Soap Cleaning: It consists of two ultrasonic baths with a ultra-pure water and two basic and acid soaps at a temperature 40-60 ^{o}C.

2. Acid Etching: It consists of etching in a solution of 0.5 Molar super-pure Nitric Acid in ultrasonic bath for half an hour at 40 ^{o}C and passivation with a solution of 10% citric acid for 1 hour at 60 ^{o}C. Then the parts must be rinsed with ultra-pure water.

8.2 Assembling

The figure 15 shows the assembling process during which all the parts of the detector have been adjusted, leaving it prepared to be attached to the magnet pipe.

8.3 Testing

Before attaching the chamber to the racket it has been made electrical and mechanical tests:

1. Electrical test: Impedance measures between high voltage parts and ground parts (see the left photo at figure 16), reaching values $\sim G\Omega$, thus assuming a good electrical isolation.

2. Vacuum test: Connection of the chamber to a vacuum pump to get a vacuum state in the part where is going to be the magnet pipe (see the right photo at figure 16). After 20 minutes pumping, a value of $5 \cdot 10^{-5}$ mbar has been reached, close to the vacuum value reached in the magnet during working time.

9. Characterization of the detector

After making electrical and mechanical tests, the next step is to characterize the detector by building two plots: electron transmission and gain curves. The electron transmission curve supplies the information of the amount of electrons which are collected from the collection zone toward the amplification zone. The gain curve supplies the information of the amount of electrons which are produced for each electron trapped at the amplification zone due to the avalanche effect.

To make this curves a flow of 2% isobutane argon is introduced through the TPC and a ^{55}Fe source is located on the PET window (on the external side of the TPC) emitting photons towards the TPC. An acquisition system called MCA (Multi Channel Analyzer) is connected to the mesh to collect the signal produced by the ions deposited at the mesh during the avalanche (see figure 11).

9.1 Electron transmission

The electron transmission curve supplies the signal information obtained from the detector depending on the ratio between the electric field applied at the TPC volume and the electric field applied at the amplification zone, that is, it is a measure of the amount of electrons which are collected from the collection zone through the mesh holes toward the amplification zone (see figure 11). This electron transmission curve is draft (see Table 2) by varying the cathode voltage and keeping the mesh voltage as constant, in this case -300 Volts. It can be observed a plateau (see figure 17) that provides a range of voltages in which the electron transmission maintains a maximum value, above 98%.

The electron transmission curve of the new detector is compared to that of the sunset Micromegas detector installed at CAST (see figure 17). SSMM have a plateau (above 98%) in a ratio (E_{drift}/E_{amp}) range of $5.5-9.5\cdot10^{-4}$, while the new SSMM have a plateau with a broader range of $7.5\cdot10^{-4}-2.5\cdot10^{-3}$. A broad plateau permits a broad variation of the electric fields without affecting the electron transmission of the detector. This behaviour of the new detector versus the electron transmission is due to the improved fabrication process, that assures a better position of the mesh holes over the tracks of the anode.

Hv Mesh: **300,0 V** Amplification gap: **5,0E-3 cm** Drift distance: **3,0 cm**

Hv Cathode (V)	E field (V/cm)	Edrift / Eamp	HV ring Top	HV ring Bottom	Peak position (channels)	Norm. Electron transmission
350,0	16,67	2,78E-04	316,7	333,3	**222,22**	0,9163
400,0	33,33	5,56E-04	333,3	366,7	**233,04**	0,9609
450,0	50,00	8,33E-04	350,0	400,0	**240,16**	0,9903
500,0	66,67	1,11E-03	366,7	433,3	**241,74**	0,9968
550,0	83,33	1,39E-03	383,3	466,7	**242,40**	0,9995
600,0	100,00	1,67E-03	400,0	500,0	**242,52**	1,0000
650,0	116,67	1,94E-03	416,7	533,3	**241,50**	0,9958

Table 2. Electron transmission data

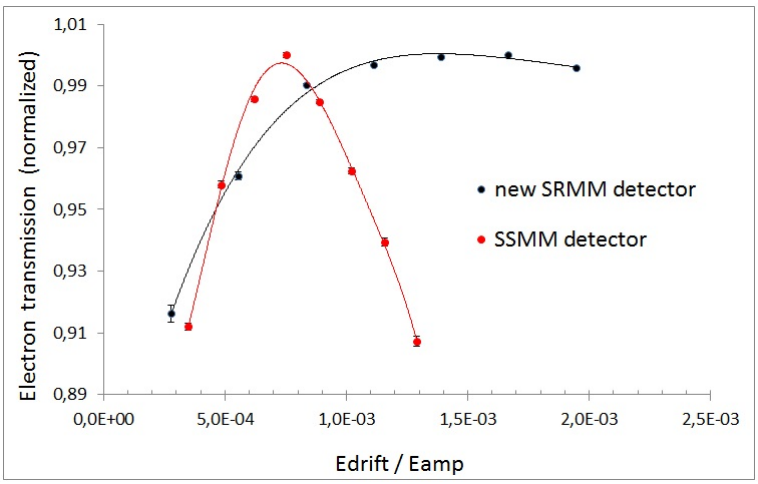

Figure 17. Electron transmission curve of the new detector.

9.2 Gain

The gain curve shows the signal depending on the electric field applied at the amplification zone, where the avalanche is produced, that is, it is a measure of the amount of electrons which are produced for each electron trapped from the TPC (see figure 11). The gain curve is draft (see Table 3) by varying the voltage at mesh and keeping the ratio E_{drift}/E_{amp} in a value that assures a maximum electron transmission, that is, within the plateau of the electron transmission curve.

As expected it is observed in figure 18 that the intensity of the avalanche effect grows with increasing the electric field E_{amp} within the amplification region. To protect the detector, to avoid sparks between mesh and anode, it is recommended to increase the electric field at the amplification region up to $60-70\ \mathrm{kV{\cdot}cm^{-1}}$, but not higher.

The gain curve of the new detector is compared to that of the sunset Micromegas detector installed at CAST (see figure 18). Both curves have an exponential behaviour, as expected, but it can be seen that the new SSMM detector have a better gain than the SRMM detectors. Overall we can say that the new detector we developed has a priori a better behaviour.

V mesh (V)	V cathode (V)	Peak position (channels)	Peak position (mV)	Peak (before TA (mV))	Peak (electrons)	Absolute gain	Eamp (kV/cm)
280,0	580,0	**110,03**	5,37E+002	8,74E+001	8,07E+005	3617,6	56
285,0	585,0	**136,58**	6,67E+002	1,08E+002	1,00E+006	4490,5	57
290,0	590,0	**155,93**	7,61E+002	1,24E+002	1,14E+006	5126,6	58
295,0	595,0	**189,61**	9,26E+002	1,51E+002	1,39E+006	6234,0	59
300,0	600,0	**233,62**	1,14E+003	1,85E+002	1,71E+006	7680,9	60
305,0	605,0	**279,5**	1,36E+003	2,22E+002	2,05E+006	9189,4	61
310,0	608,0	**337,55**	1,65E+003	2,68E+002	2,48E+006	11097,9	62
315,0	608,0	**421,89**	2,06E+003	3,35E+002	3,09E+006	13870,9	63

Table 3. Gain data

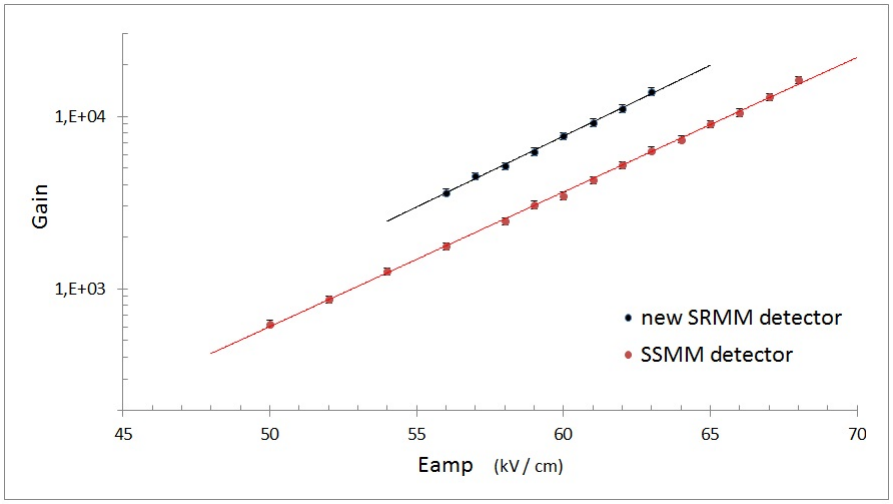

Figure 18. Gain curve of the new detector.

9.3 Spatial reconstruction

In section 7.4.2 the working principle of T2K system was explained. This system is based on the integration of the chip called AFTER at the FEC cards, which amplifies and digitalizes the signal coming from each track of the Micromegas and records them in 511 temporal channels (time bin). In this case each channel has been adjusted to 10 ns, thus recording 5.110 ns per event, time enough to recover all the electrons produced by a photon trace in the TPC. Thus a pulses pattern as figure 19 (top left) is recover for each trace. The trigger for each event recording is made when a threshold, imposed manually, is exceeded at the mesh, thus an undesired background recording is avoided.

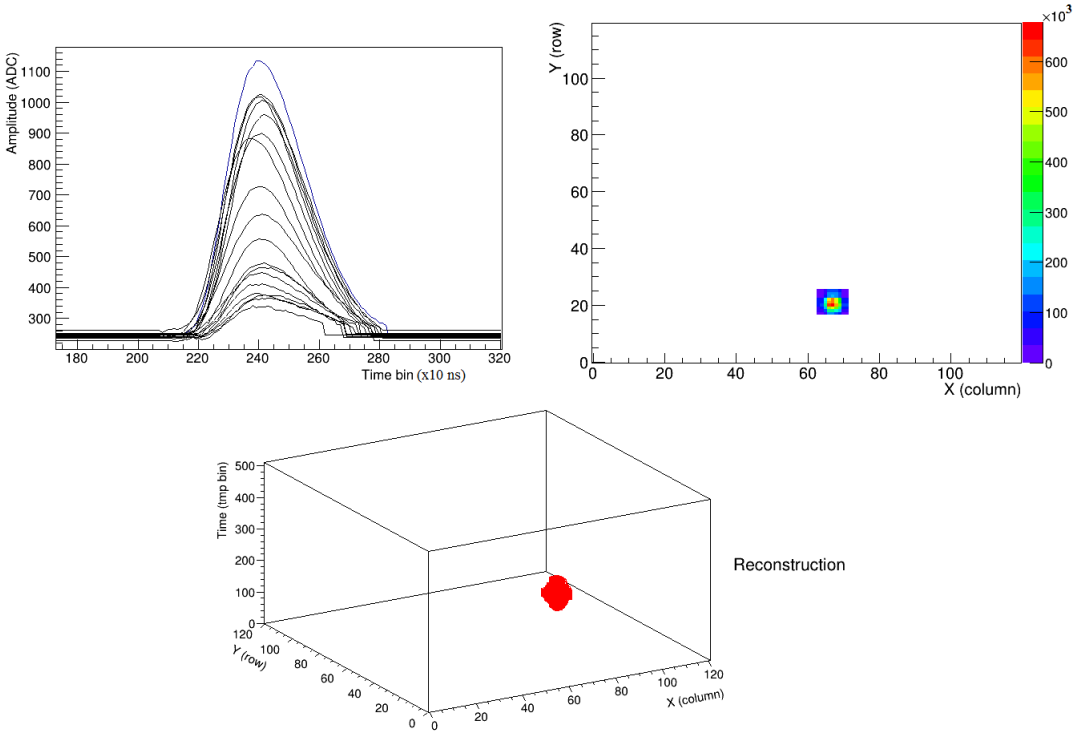

Figure 19. Top left: pulses recorded by the T2K system for an event. Each pulse correspond to a track at the Micromegas circuit. The X axis represents the trigger time and the Y axis represents the signal amplitude. **Top right**: 2D distribution of the Micromegas plane for the event recorded at the left. **Down**: 3D reconstruction of the event.

The figure 20 shows a 2D event distribution on the Micromegas. Putting attention it is possible to distinguish the grill of the strong-back. The left figure shows the full area with the electric field guide switched off, thus the strong-back lines yields deviated from straight due to the effect of the contour. This effect disappears in the center figure where the electric field guide is switched on, getting an electric field uniform and vertical as desired. The right figure shows the same event distribution as before but the source is collimated on the center of the PET window using an aluminium piece with a small hole put under the source. This time most of the events are collected on the center of the Micromegas, as desired. No more studies on the events distribution have been made, but it would be interesting to do a statistical study collimating the source on several zones at the Micromegas to test the behaviour on all the zones.

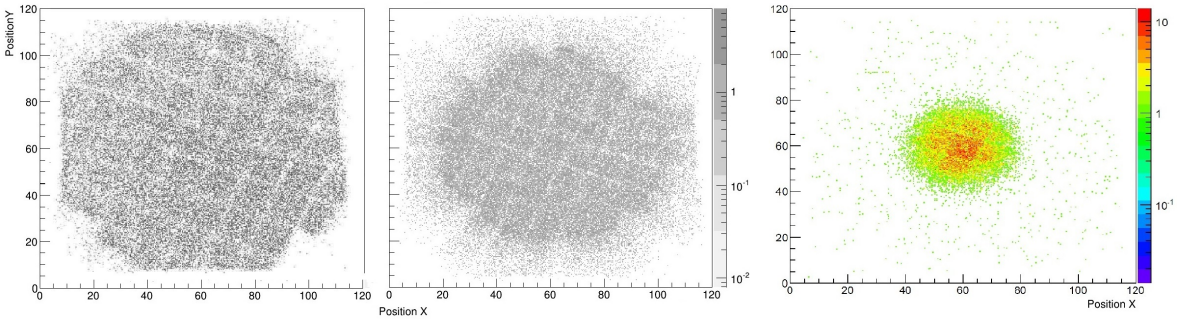

Figure 20. 2D distribution of the Micromegas. **Left**: full area with the electric field guide switched off. **Center**: full area with the electric field guide switched on. **Right**: Source collimated on the center.

10. Next steps and prospects on the new detector

Next step for the sunrise new detector, after its mounting and characterization, is to calibrate it by using a X-ray generator which is available in the laboratory of CAST at CERN. This step is already done and at the moment of delivering this master project the sunrise new detector is already in commissioning phase at the magnet.

Apart from this detector developed here, this commissioning is made up of several new improvements which some of them have been explained before. It is planned that the experiment is ready for taking data at the end of this very month, September 2013, and it will be working until the end of this very year. For the next year is planned to fabricate a new sunrise detector with the same improvements than developed here but taking into account the fabrication and mounting of the new improved X-ray optics, which is at this moment in design phase (see section 5.2).

It is hard to make a precise estimation of the achievable background by CAST 2013 detectors, however clear hints of the potential improvement can been found from underground measurements and surface tests carried out in Zaragoza and Saclay, and with 2012 SSMM. The results are summarized in the Figure 21.

The red points correspond to background measurements done in the Canfranc Underground Laboratory. The improvement along the series is due exclusively to external shielding upgrades. The same strategy yields more modest results at surface (blue points). The difference should be attributed to cosmic rays. In fact, the last and lowest two points of the blue series show the effect of the preliminary installation of a cosmic veto over SSMM detectors. The green dots are simulation results using external gamma environmental flux as the only background source. Later, simulation values have been added to the unavoidable background contribution by intrinsic radioactivity of detectors, which had been evaluated in Canfranc. The simulation results are taken as a model to deduce the effect on the background of the screening of the environmental gamma flux as a function of the shielding thickness: the green line that it is a fit on the simulation values using a double exponential over the intrinsic background level deduced from underground tests. The plot shows that this behaviour perfectly explains the underground series.

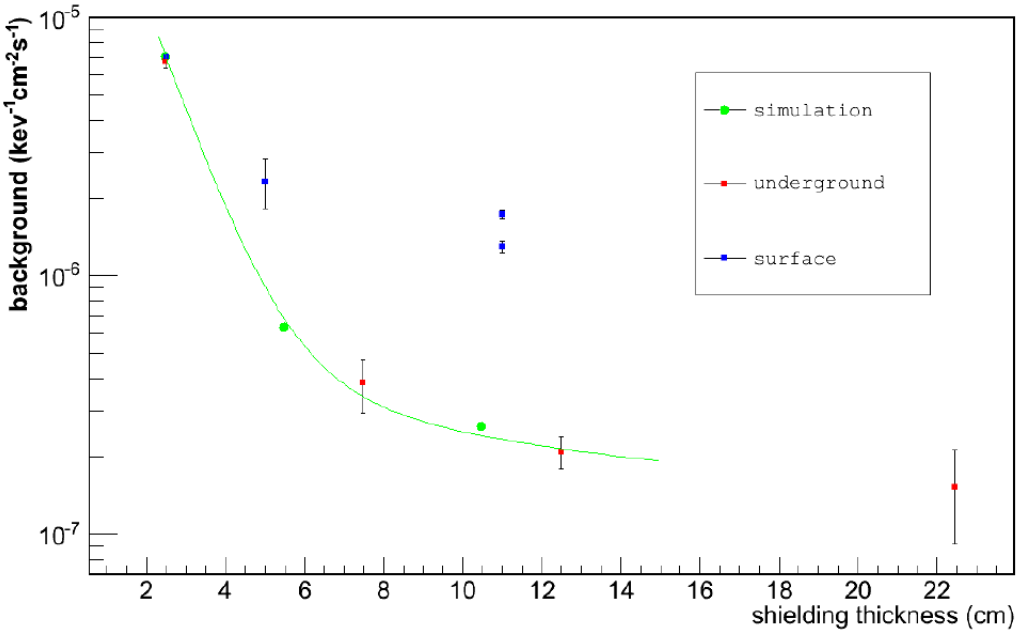

Figure 21. Shielding test underground and at surface together with Monte Carlo simulation expectation.

Therefore the green line can be used as a background expectation in the ideal case where the cosmic rays contribution could be completely removed. For present SSMM, with 10 cm lead shielding, it is around $3{\cdot}10^{-7}$ s^{-1} keV^{-1} cm^{-2} cast-units; while for the new SRMM, the lead shielding thickness is still undefined and could be, in the worse case, 5 cm, and therefore around $7{\cdot}10^{-7}$ cast-units. It should not be forgotten that there are another contributions to the background due to the presence of shielding weak points in the connection of detectors to the magnet and the extraction of the signals.

But from the present evidence of cosmic veto efficiency, with coverage factors which can still be notably improved, and the big margin with respect to underground levels point to future Micromegas backgrounds to descend comfortably below the $1{\cdot}10^{-6}$ cast-units barrier in both sunset and sunrise sides.

11. Conclusions

Along this master project I have presented my work, done during a year, involved on the design and construction of the new detector for CAST, while I learnt at the same time on the physics behind this experiment and on the whole particle physics experiments.

We started to see a brief introduction to the axion world, where the existence of axion was theoretically explained as solution of the strong CP problem. This solution is beyond the standard model of particles and, if confirmed, will force the revision of this standard model so established among the scientific community. Then we saw the theoretical axion properties, its interactions with ordinary matter and the axion emission processes, and only interactions with photons through the Primakoff process are taken into account in CAST experiment and in most of the experiments in searching for axions.

The axion, as dark matter candidate, satisfy the criteria for cold dark matter, and the confluence of laboratory, cosmological and astrophysical constraints restrict the axion mass range in $\sim$mV. However CAST is currently sensitive to axions only at somehow higher masses $\sim 0.1-1$ eV, therefore in this range the axions would rather contribute to hot dark matter.

Beyond the dark matter problem, which could be solved by theoretically motivated particles such as axions and WIMPs, the problem of the dark energy lacks however such well-motivated solutions. Either explanation involves "new physics", some of which can be investigated in parallel with dark matter by using existing experiments in astroparticle physics as CAST and other disciplines. Also it is intriguing that the possible detection of ALPs, another motivation for CAST experiment, might become the key to the much sought experimental test of string theory.

Independently of the theoretical framework behind, the proposed experimental improvement of CAST will open a completely new observational window for WISPs in the sub-keV range, previously unexplored. It is considered the possibility of using such a unique setup like CAST, enhanced with sensitivity in a new energy window, is by itself worthwhile pursuing.

One of the innovations in which CAST success has relied, apart from the availability of a high class magnet like the LHC superconducting test magnet and low background techniques, is the use of X-ray optics to focus the beam and increase the signal-to-noise ratio. The building of this optics is delayed and at this moment it is at design phase, and it is planned to be mounted on CAST for the next year. The new SSMM detector developed here is mounted on CAST for testing its behaviour after the improvements implemented and it will be used for validating the 2014 final setup.

Micromegas technology is applied by the CAST team from earlier detectors and every day the knowledge of this technology is growing, thus it permits a better detectors development. Although the new SSMM detector did not take data yet, we presume that it will exceed to the previous detectors, and not only due to the own configuration but too because of the improvements developed to the equipment sited around it, as shielding, read out, optics and others.

The expected new CAST results will be important input also for the IAXO proposal, since all the experience and knowledge accumulated by CAST will be used to design and develop the IAXO experiment.

12. Acknowledgements

First of all I would like to thanks to Igor Irastorza, director of this master project, not only for the guide of my work but even because the opportunity of being part of the GIFNA group (Grupo de Investigación en Física Nuclear y Astropartículas).

The first time I took contact to the CAST experiment was in September 2012, when Juan Castel gave me the drawings of the previous detectors which he had developed. From then until the end, he has been helping me in all the moments I needed. Later Juan Antonio García and Javier Gracia started to help me with the new design, telling me their experience in the CAST experiment and other experiments in searching for rare events, above all they advised me on the radio-purity techniques (later I learnt more on it in the Underground Laboratories course).

During the project meetings, people of the team as Paco or Alfredo started to give me ideas on the design, and later Francisco Aznar, the electronic expert, made all the design of the Micromegas circuit according to the TPC design, and sure he remember the last minute changes which forced

him to redesign and redesign the circuit, until we made the order to the workshop at the beginning of February 2013.

The parts fabrication were made most of them by the precision mechanic workshop of the university of Zaragoza and by Angel Lagraba in the workshop of the group. I want to thank to Angel for his infinite patient and always good disposition, in spite we had a delay of two months and during all the month of May I was asking and asking for pieces.

In June 2013 I had the great opportunity of going to the CERN to mount the detector and to make the first tests of characterization, since the Micromegas workshop is there too. I will foundly remember this trip with my colleges Juan, Javier and Theopisti... great!. I want to thanks to Theopisti Dafni who took me to all the buildings I needed and introduced me to the scientific community there.

During the redaction of this master project my colleges are at CERN mounting the detectors in the magnet. I can not be there despite I would like so much, only I hope that everything goes well and we have the CAST telescope running as soon as possible, facing the sun and catching everything that the human eye can not catch.

References

[1] Michael S. Turner, *Windows on the axion*, Fermilab Conference 1989.

[2] Jihn E. Kim et al, *Axion and the strong CP problem*, Review of modern physics 2010.

[3] L.D. Duffy, *Axions as dark matter particles*, New Journal of Physics 11-105008 (2009).

[4] L. Visinelli and P. Gondolo, *Dark Matter Axions Revisited*, arXiv: 0903.4377v2 20 Oct (2009).

[5] L.D. Duffy, P. Sikivie and D.B. Tanner, *High resolution search for dark-matter axions*, Phys.Rew. D 74, 012006 (2006).

[6] P. Sikivie and Q. Yang, *Bose-Einstein Condensation of Dark Matter Axions*, arXiv:0901.1106v4 2 Sep (2009).

[7] J.P. Conlon, M.C.D. Marsh, *The Cosmophenomenology of Axionic Dark Radiation*, arXiv: 1304.1804v1 (2013).

[8] I.G.Irastorza, et. al., *The International Axion Observatory (IAXO)*, arXiv:1201.3849

[9] Z. Ahmed et al, *Search for Axions with the CDMS Experiment*, Phys. Rew. Lett. 103, 141802 (2009).

[10] M. Sulc et al, *Axion search by laser-based experiment OSQAR*, Nucl. Instr. Meth. in Phys. Research (2012).

[11] Robin Bährea, et al, *Any Light Particle Search II Technical Design Report*, arXiv:1302.5647v2 [physics.ins-det] 2 Aug 2013.

[12] *Web page of the PVLAS experiment* http://pvlas.ts.infn.it/physics.html.

[13] *Web page of the ADMX experiment* http://www.phys.washington.edu/groups/admx/home.html.

[14] *Web page of the CAST experiment* http://cast.web.cern.ch/CAST/index.php.

[15] Yoshizumi Inoue et al, *Status report of the Tokyo axion helioscope experiment*, Journal of Physics: Conference Series 120 042014 (2008).

[16] Wei Liao, *Generation and search of axion-like light particle using intense crystalline field*, Phys. Lett. B 702 55–58 (2011).

[17] S.A. Hoedl et al, *A torsion pendulum based axion search*, Physics Procedia 17 96–99 (2011).

[18] O.K. Baker et al, *Prospects for Searching Axion-like Particle Dark Matter with Dipole, Toroidal and Wiggler Magnets*, arXiv:1110.2180v1 (2011).

[19] A.B. Balakin and L.V. Grunskaya, *Axion electrodynamics and dark matter fingerprints in the terrestrial magnetic and electric fields*, Reports on Mathematical Physics Vol. 71 (2013).

[20] E. Arik et et al. [CAST Collaboration], *Probing eV-scale axions with CAST*, JCAP 0902, 008 (2009) [arXiv:0810.4482 [hep-ex]]

[21] K. Zioutas et al. [CAST Collaboration], *First results from the CERN Axion Solar Telescope (CAST)*, Phys. Rev. Lett. 94, 121301 (2005) [hep-ex/0411033].

[22] S. Andriamonje et al. [CAST Collaboration], *An Improved limit on the axion-photon coupling from the CAST experiment*, JCAP 0704, 010 (2007) [hep-ex/0702006].

[23] G. Luzon et al, *Background studies and shielding effects for the TPC detector of the CAST experiment*, New Journal of Physics 9, 208 (2007).

[24] P. Arias, D. Cadamuro, M. Goodsell, J. Jaeckel, J. Redondo, et. al., *WISPy Cold Dark Matter*, arXiv:1201.5902

[25] F. J. Iguaz et al, *Ultralow background periods in CAST Micromegas detectors and tests in the Canfranc Underground Laboratory*, J. Phys.: Conf. Ser. 309 012002 (2011).

[26] N. Abgrall et al, *Time Projection Chambers for the T2K Near Detectors*, Nuclear Instruments and Methods in Physics Research Section A. Volume 637, 25–46 (2011).